Effect of Neodymium and Transition Metals Co-doped on Structural, Optical and Magnetic Properties of BiFeO$_3$ Materials

Dao Viet Thang[1,2,*], Du Thi Xuan Thao[2], Le Thi Mai Oanh[1], Nguyen Van Minh[1]

[1]*Center for Nano science and Technology, Hanoi National University of Education,*
136 Xuan Thuy, Hanoi, Vietnam
[2]*Department of Physics, Hanoi University of Mining and Geology,*
Duc Thang, Bac Tu Liem, Hanoi, Vietnam

Abstract: Structural, optical and magnetic properties of BiFeO$_3$ and Bi$_{0.9}$Nd$_{0.1}$Fe$_{0.95}$TM$_{0.05}$O$_3$ (TM = Ni, Co) polycrystallines prepared by sol–gel method have been investigated. X-ray diffraction (XRD) patterns reveal that all samples crystalize in rhombohedrally distorted perovskite structure belonging to R$_{3C}$ space group. The analysis results of both XRD and Raman scattering show the increase of lattice distortion with the co-replacing of Nd and TM ions into A and B sites respectively. All samples exhibit a weak ferromagnetic behavior at room temperature with the enhancement of the magnetization in Nd and TM co-doped samples.
Keywords: Raman, co-doped, magnetization, BFO.

1. Introduction

Due to the simultaneous coexistence of ferroelectric, ferromagnetic and ferroeleastic phase, multiferroics materials recently are interested in many research groups all over the world. This kind of materials promises the application in novel devices such as spintronics, information storage, sensing and actuator [1, 2]. Among the multiferroics, BiFeO$_3$ (BFO) has been regarded as one of the most widely studied single-phase multiferroics showing multiferroics properties at room-temperature, T_C at 1103 K and T_N at 643 K [3, 4]. BFO is crystallized in a rhombohedrally distorted perovskite ABO$_3$ structure belonging to R$_{3C}$ space group. The stereochemical activity of Bi 6s^2 lone-pair electrons, hybridized with both the empty 6p^0 orbitals of Bi^{3+} ion and the 2p^6 states of O^{2-} ion is responsible for non-centrosymmetric ferroelectric order along the <111> direction of the cubic perovskite-like lattice [3, 5, 6]. On the other hand, the magnetic structure of BFO shows G-type anti-ferromagnetism order modulated by a cycloid spin below the Néel temperature [6, 7]. However, bulk

_____
* Corresponding author. Tel.: 84-:985811377
  Email: daoviethang@humg.edu.vn

BFO is not suitable for device applications because the appearance of impurity phases in bulk sample leading to a high leakage current, a weak ferromagnetic ordering, and a wide range change of transition temperature [3, 8, 6]. In order to solve these problems, a chemical modification doping rare earth or transition metals ions into A- or B-sites of the perovskite BFO is strongly recommended [9, 10]. Many works reported the enhancement of electrical and magnetical properties of BFO material. Which the A-sites are replaced by trivalent rare earth ions (Nd^{3+}, La^{3+}, Ho^{3+}, Sm^{3+}, Eu^{3+}, Gd^{3+}) [11-16, 10, 17] or divalent metal ions (Ba^{2+}, Sr^{2+}, Ca^{2+}, Pb^{2+}) [18-21] and B-sites are substituted by some transition metal cations (Zr^{4+}, Nb^{5+}, Ni^{2+} or Co^{2+}) [22-26]. The magnetoelectric effect in these materials was assigned to the coupling between ferroelectric order resulting from electron lone pair of A-site Bi^{3+} ions and the ferromagnetic order resulting from the substitution of cation Fe^{3+} into B-site [27].

In this study, neodymium and transition metals co-doped BFO samples were synthesized by sol-gel method. The influence of neodymium and transition metals co-doped on the microstructures, surface morphology, magnetic and optical properties of materials were investigated.

2. Experimental

$BiFeO_3$ (BFO), $Bi_{0.9}Nd_{0.1}FeO_3$ (BNFO), $Bi_{0.9}Nd_{0.1}Fe_{0.95}Ni_{0.05}O_3$ (BNFNO) and $Bi_{0.9}Nd_{0.1}Fe_{0.95}Co_{0.05}O_3$ (BNFCO) nanocrystals were prepared by sol–gel method. For preparation of precursor solutions, $Nd(NO_3)_3.6H_2O$, $Bi(NO_3)_3.5H_2O$, $Fe(NO_3)_3.9H_2O$, $Ni(NO_3)_2.6H_2O$, and $Co(NO_3)_2.6H_2O$ were used as starting materials. In the first step, these chemicals were mixed in correct weight contribution and an aqueous solution of citric acid and ethylence glycol was prepared in distilled water. Then, salt of iron nitrate, bismuth nitrate, neodymium nitrate and nickel(II) nitrate (or cobalt(II) nitrate) were added in turn with constant stirring at temperature 50 – 60 °C to avoid precipitation and obtain a homogeneous solution. Solution of citric acid and ethylene glycol was dropped into the solution with the molar ratio of citric acid/ethylene glycol of 70/30. Then, water in solution was evaporated at temperatures 100 °C to obtain colloidal gel. Finally, the gel was heat treated at temperature of 800 °C for 7 hours to remove organics in the samples and crystalize $BiFeO_3$ nanocrystal.

The samples were characterized by different techniques: X-ray diffraction pattern using a D5005 diffractometer with CuKα radiation and with 2θ varied in the range of 20 – 70° at a step of 0.03°. Raman scattering measurements were performed by Jobin Yvon T64000 spectrometer equipped with wavelength 514.5 nm of Ar laser. The surface morphology was explored by scanning electron microscopy. The optical and electrical properties were determined by the absorption spectra using a Jasco V670 UV-VIS photospectrometer. Vibrating sample magnetometer was used to measure magnetic properties of the samples

3. Results and discussion

Fig. 1a shows XRD patterns of the BFO, BNFO, BNFNO and BNFCO samples. Impurities phases are not detected in BFO and BNFO samples but they are found in BNFNO and BNFCO samples. BFO

sample shows the strong separation of (104)-(110) diffraction peak couple (the small Figure). For co-doped samples, these peaks shift closer together and tend to merge into a single peak. The ratio of diffraction intensity between (104) and (110) peaks decreases rapidly from 1.04 to 0.82. Moreover, almost of XRD peaks shift toward the higher value of 2θ angle. These changes in XRD patterns indicate that the lattice parameters of the BNFO, BNFNO and BNFCO samples are altered by doping especially in co-doping samples. The values of lattice parameters were calculated by UnitCell software and displayed in Fig. 1b. This change could be attributed to the difference of ion radius between the host lattice ions Bi^{3+} and Fe^{3+} to replacing ions Nd^{3+} and Ni^{2+} (Co^{2+}) respectively [27].
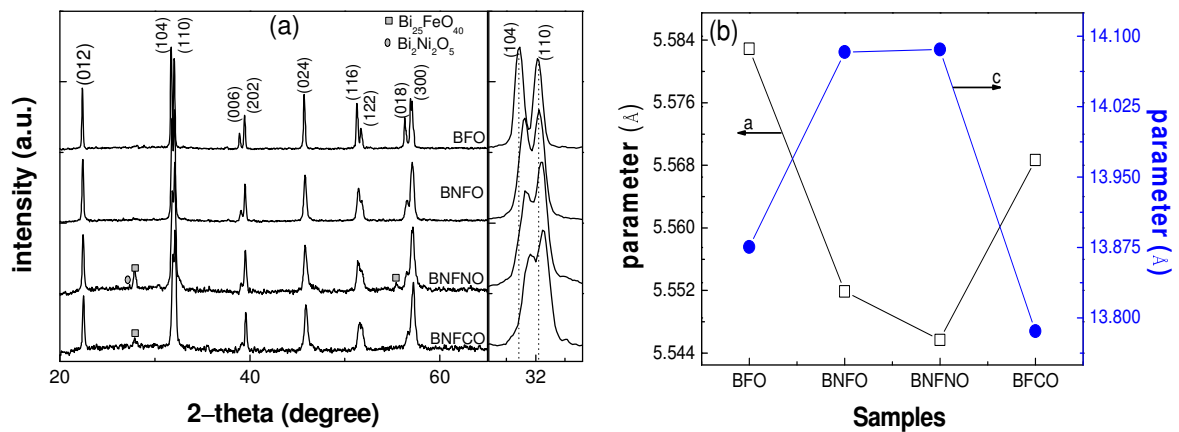

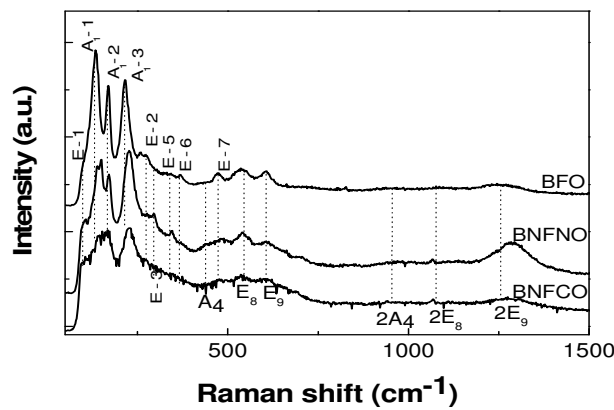Fig. 1. XRD patterns of the BFO, BNFO, BNFNO and BNFCO powders.

Fig. 2. Raman spectra of BFO, BNFNO and BNFCO powders at room temperature.

The structural transformation of BNFNO and BNFCO materials are also observed in Raman spectra. Fig. 2 shows the Raman spectra of BFO, BNFNO, and BNFCO samples. According to group theory, there are 13 Raman-active modes predicted for the rhombohedrally distorted space group R_{3C}, which can be summarized using the following irreducible representation: $\Gamma = 4A_1 + 9E$, including A_1-1, A_1-2, A_1-3 and A_1-4 modes at 136, 168, 212 and 425 cm^{-1}, respectively, and E modes at 71, 98, 275,

305, 335, 363, 456, 549 and 597 cm^{-1} [28, 29]. As shown in Fig. 2, the observed Raman spectral containing 11 peaks of pristine sample is in good agreement with the results reported by Yuan *et al.* [29] and Singh *et al.* [28]. Three intense peaks at 132, 169 and 215 cm^{-1} are assigned to A_1-1, A_1-2 and A_1-3 modes, respectively. The other eight peaks at 96, 270, 338, 368, 436, 470, 544 and 605 cm^{-1} are assigned to E-1, E-2, E-5, E-6, A_1-4, E-7, E-8 and E-9 modes, respectively. It is interesting to note that the E-3 modes at 293 cm^{-1} is detected in BNFNO sample which is not observed in the BFO and BNFCO samples. Although the result is not reported, this peak may cause of from the impurity $Bi_2Ni_2O_5$ phase (it is suitable with RXD result in Fig.1). However, it needs evidences to clarify this issue. For BFO sample, E-2 mode at 270 cm^{-1} and A_1 modes at 132, 169 and 215 cm^{-1} in the low frequency range are associated with Bi-O vibration. High frequency E modes correspond to Fe-O vibration [29, 30]. Co-doped samples (BNFNO and BNFCO) exhibit the shift of three Raman modes A_1-1, A_1-2 and A_1-3 to higher frequency. The changes of both intensity and position of these peaks indirectly indicates the substitution of Nd^{3+} ions for Bi^{3+} ions [7]. Moreover, the shift of E-3 and E-8 modes to higher frequency reveals the increase of local lattice distortion and the formation of oxygen vacancy due to substitution of the Ni, Co dopant at the B site [7, 31]. Compressive stress of structural distortion due to co-doping. The appearance of a prominent additional band around ~ 1000 – 1350 cm^{-1} in co-doped samples can be assigned to the two-phonons Raman scattering in BFO labeled as $2A_4$, $2E_8$ and $2E_9$ [30]. The strong contribution of these two-phonon bands to the total Raman spectrum has been attributed to a resonant enhancement with the intrinsic absorption edge in BFO [32, 33].
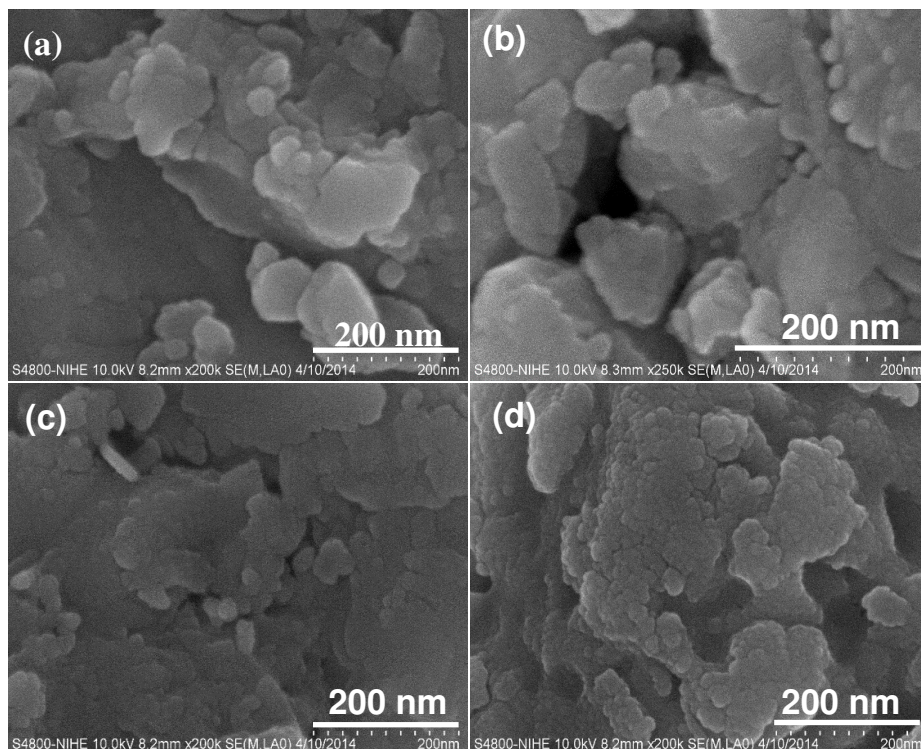

Fig. 3. (a)-(d) SEM images of the BFO, BNFO, BNFNO and BNFCO materials, respectively.

Fig. 3 presents SEM images of four study samples which exhibit the sphere particle grain shape. The particles size are evaluated varying from 40 to 100 nm for BFO sample. The particle size generally decreases in doped and co-doped samples comparing to un-doped BFO sample. This can be explained by the replacing of dopant ions into BFO lattice crystal. This causes the crystal distortion and limits the growth of crystal.

Fig. 4a shows UV–Vis absorption spectrum of BFO, BNFO, BNFNO and BNFCO samples (insert figure is the plots of $(\alpha h\nu)^2$ versus $(h\nu)$ for the BFO sample). The band gap values obtained by Wood-Tauc method for BFO, BNFO, BNFNO and BNFCO samples are 2.03, 2.00, 1.97, and 1.85 eV, respectively (in Fig. 4b). The valence band of BFO material are well known forming by 3d-Fe and 2p-O states. The conduction band is composed of 3d-Fe and 6p-Bi states. The appearance of second absorbance at 700 nm can be assigned to the transition of electron from t_{2g} bands to e_g bands of Fe^{3+} ions [34, 35]. The slight decrease of optical band gap in doped and co-doped samples can be explained by the appearance of Nd impurity band in the energy band gap. Fig. 4a also exhibit a weak absorption peak at 750 nm for doped and co-doped BFO samples which can be assigned to electron transitions from the ground state $^4I_{9/2}$ to the excited levels $(^4F_{7/2} + {}^4S_{3/2})$ of Nd^{3+} ion [36].
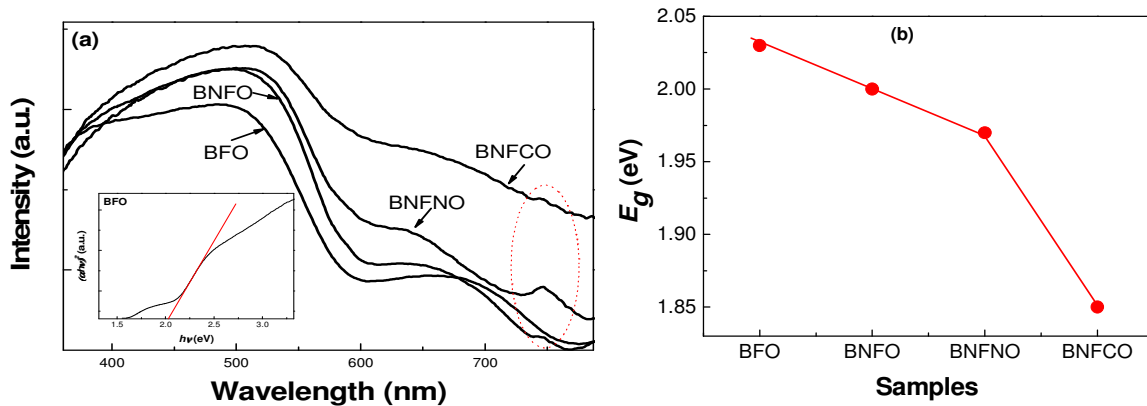

Fig. 4. (a) UV–Vis absorption spectrum of the BFO, BNFO, BNFNO and BNFCO samples. The insert shows the plot of $(\alpha h\nu)^2$ as a function of photon energy of the BFO. (b) optical band gap of the samples, respectively.
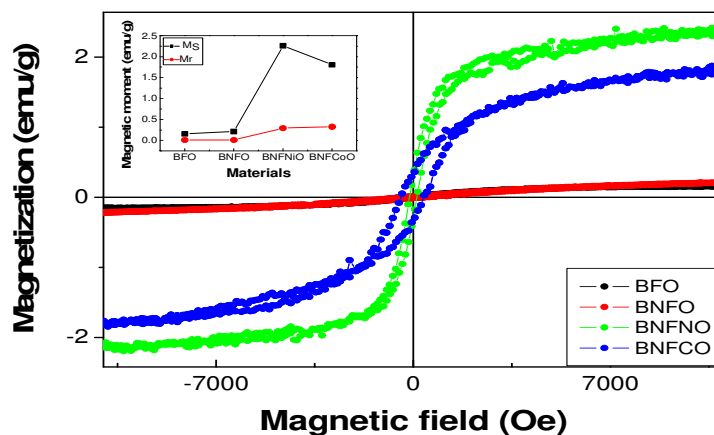

Fig. 5. Magnetic-field dependence of the magnetization for BFO, BNFO, BNFNO and BNFCO materials.

Fig. 5 presents the magnetic hysteresis (M-H) loops of the BFO, BNFO, BNFNO and BNFCO samples under the maximum field of 10 kOe at room temperature. It is clear that all samples display a weak ferromagnetic behavior. The magnetizations sharply increase in co-doped BFO samples comparing to un-doped and Nd-doped BFO samples. The calculated saturation magnetization values of the BFO, BNFO, BNFNO and BNFCO samples are 0.155, 0.211, 2.262 and 1.808 emu/g, respectively. Yoo *et al.* [7] reported that the enhanced magnetic moment of co-doped samples can be assigned to the transition of magnetic structure from incommensurate cycloidal spiral spin structure to G-type collinear antiferromagnetic structure.

4. Conclusions

The doped, co-doped and un-doped $BiFeO_3$ materials were prepared by sol–gel method. The replacement of Nd into A-sites and Co (Ni) into B-site were observed through the shift of XRD peaks resulting the change of lattice parameters and the shift of Raman peaks which related to the vibration of replacing sites. The optical band gap changes with the co-substitution of rare earth and transition metal into BFO crystal lattice. Weak ferromagnetism was observed in all samples with the sharply increase of saturation magnetization values H_C in co-doped BFO samples comparing to un-doped BFO and Nd-doped BFO samples.

Acknowledgments

Reference

[1] Eerenstein W., N.D. Mathur, and J.F. Scott, Nature. 442, (2006) 759-765.

[2] Tokura Y., J. Magn. Magn. Mater. 310, (2007) 1145–1150.

[3] F. Kubel and H. Schmid, Acta Cryst. B46, (1990) 698-702

[4] X. Qi, J. Dho, R. Tomov, M. G. Blamire, and J.L.M. Driscoll, Appl. Phys. Lett. 86, (2005) 062903.

[5] P. Ravindran, R. Vidya, A. Kjekshus, H. Fjellvåg, and O. Eriksson, Phys. Rev. B 74, (2006) 224412.

[6] X.J. Xi, S.Y. Wang, W.F. Liu, H.J. Wang, Feng Guo, Xu Wang, J. Gao, and D.J. Li, J. Mag. Mag. Mater. 355, (2014) 259–264.

[7] Y.J. Yoo, J.S. Hwang, Y.P. Lee, J.S. Parkb, J.Y. Rhee, J.-H. Kang, K.W. Lee, B.W. Lee, and M.S. Seo, J. Magn. Magn. Mater. 374, (2015) 669–675.

[8] B. Ruette, S. Zvyagin, A. P. Pyatakov, A. Bush, J. F. Li, V. I. Belotelov, A. K. Zvezdin, and D. Viehland, Phys. Rev. B. 69, (2004) 064114.

[9] Lazenka V.V., A.F. Ravinski, I.I. Makoed, J. Vanacken, G. Zhang, and V.V. Moshchalkov, J. Appl. Phys. 111(12), (2012) 123916.

[10] K. Chakrabarti, K. Das, B. Sarkar, and S.K. De, J. Appl. Phys. 110, (2011) 103905.

[11] M.S.B. Darby, D.V. Karpinsky, J. Pokorny, S. Guerin, A.L. Kholkin, S. Miao, B.E. Hayden, and I.M. Reaney, Thin Solid Films. 531, (2013) 56-60.

[12] G. L. Yuan, Siu Wing Or, J. M. Liu, and Z.G. Liu, Appl. Phys. Lett. 89, (2006) 052905

[13] Sen K., S. Thakur, K. Singh, A. Gautam, and M. Singh, Mater. Lett. 65(12), (2011) 1963-1965.

[14] Raoa T.D., T. Karthika, A. Srinivasc, and S. Asthanaa, Solid State Commun. 152(23), (2012) 2071–2077.

[15] Xu X., T. Guoqiang, R. Huijun, and X. Ao, Ceram. Int. 39(6), (2013) 6223-6228.

[16] Minh N.V. and D.V. Thang, J. Nonlinear Opt. Phys. 19(2), (2010) 247–254.

[17] Lotey G.S. and N.K. Verma, Chem. Phys. Lett. 574, (2013) 71-77.

[18] Chauhan S., M. Arora, P.C. Sati, S. Chhoker, S.C. Katyal, and M. Kumar, Ceram. Int. 39(6), (2013) 6399-6405.

[19] Wang L.Y., D.H. Wang, H.B. Huang, Z.D. Han, Q.Q. Cao, B.X. Gu, and Y.W. Du, J. Alloy. Compd. 469(1-2), (2009) 1-3.

[20] Tirupathi P. and A. Chandra, J. Alloy. Compd. 564, (2013) 151-157.

[21] R. Mazumder and A.Sen, J. Alloy. Compd. 457, (2009) 577–580.

[22] Xie J., Y. Liu, C. Feng, and X. Pan, Mater. Lett. 96, (2013) 143-145.

[23] Jun Y.-K., W.-T. Moon, C.-M. Chang, H.-S. Kim, H.S. Ryu, J.W. Kim, K.H. Kim, and S.-H. Hong, Solid State Commun. 135(1-2), (2005) 133-137.

[24] Wen Z., G. Hu, S. Fan, C. Yang, W. Wu, Y. Zhou, X. Chen, and S. Cui, Thin Solid Films. 517(16), (2009) 4497-4501.

[25] Y.R. Dai, Qingyu Xun, Xiaohong Zheng, Shijun Yuan, Ya Zhai, and M. Xu, Physica B 407, (2012) 560–563.

[26] Lin Peng, Hongmei Deng, Jianjun Tian, Qing Ren, Cheng Peng, Zhipeng Huang, Pingxiong Yang, and J. Chu, Appl. Surf. Sci. 268, (2013) 146– 150.

[27] K. Chakrabarti, K. Das, B. Sarkar, S. Ghosh, and S.K. De, Appl. Phys. Lett. 101, (2012) 042401.

[28] Singh MK, Jang HM, Ryu S, and J. MH, Appl. Phys. Lett. 88, (2006) 042907-042907-3.

[29] G. L. Yuan, S. W. Or, and H.L. Chan, J. Appl. Phys. 101, (2007) 064101.

[30] Xia Yan, Guoqiang Tann, Wenlong Liu, Huijun Ren, and A. Xia, Ceram. Int. 41, (2015) 3202–3207.

[31] Hermet P., M. Goffinet, J. Kreisel, and P. Ghosez, Phys. Rev. B. 75(22), (2007).

[32] Ramirez M.O., M. Krishnamurthi, S. Denev, A. Kumar, S.-Y. Yang, Y.-H. Chu, E. Saiz, J. Seidel, A.P. Pyatakov, A. Bush, D. Viehland, J. Orenstein, R. Ramesh, and V. Gopalan, Appl. Phys. Lett. 92(2), (2008) 022511.

[33] Minh N.V. and D.V. Thang, J. Alloy. Compd. 505(2), (2010) 619-622.

[34] Liu Z., Y. Qi, and C. Lu, J. Mater. Sci.-Mater. El. 21(4), (2009) 380-384.

[35] Thang; D.V., D.T.X. Thao;, and N.V. Minh, J. Sci. Tech. 52(3C), (2014).

[36] Bagayev S.N., V.V. Osipov, M.G. Ivanov, V.V. Platonov, A.N. Orlov, A.V. Spirina, S.M. Vatnik, and A.S. Kaygorodov, Laser Phys. 19(5), (2009) 1165-1168.